Anal. Bioanal. Electrochem., Vol. 15, No. 12, 2023, 1098-1115
https://www.doi.org/10.22034/abec.2023.709690

Analytical &
Bioanalytical
Electrochemistry

2023 by CEE
www.abechem.com

Full Paper

Combination of G-C_3N_4 and Triplex Metal Oxides for Enhanced Performance of Oxygen Reduction Reaction

Seyed Sina Hosseini,[1,2] Mehdi Mehrpooya,[1,2,*] and Mohammad Hossein Jahangir[1]

[1] *Faculty of New Sciences and Technologies, University of Tehran, Tehran, Iran*
[2] *Hydrogen and Fuel Cell Laboratory, Faculty of New Sciences and Technologies, University of Tehran, Tehran, Iran*

*Corresponding Author, Tel.: +982188497167
E-Mail: mehrpoya@ut.ac.ir

Received: 25 November 2023 / Received in revised form: 23 December 2023 /
Accepted: 27 December 2023 / Published online: 31 December 2023

Abstract- Given the rising concerns regarding climate change, there has been a noticeable rise in research dedicated to exploring materials aimed at bolstering the efficiency of energy conversion technologies, like fuel cells. The development of efficient and affordable non-precious electrocatalysts for the oxygen reduction reaction (ORR) is vital for the advancement of fuel cells. In this study, we synthesized a new hybrid catalyst for ORR consisting of triple Metal Oxide (IIIMO) decorated on a porous graphitic carbon nitride (PCN); as well, its physiochemical and electrochemical performance was assessed. This composite facilitates a synergistic enhancement of catalytic activity for the ORR, benefiting from its binary composition and hierarchically porous structure. The synthesis of the PCN-IIIMOx% composite employed a straightforward layer-by-layer assembly method, integrating several weight ratios of IIIMO (where x represents 10, 20, 50, and 100%). The physiochemical analyses confirmed the incorporation of the as-synthesized IIIMO on the PCN lattice. The electrochemical analyses showed that the PCN-IIIMO20% has the best performance holding the onset potential of -0.09 V, electron transfer number of 3.3, and current retention durability of 79% after 7200s of continuous operation.

Keywords- Oxygen reduction reaction; Non-precious electrocatalyst; Porous graphitic carbon nitride; Triple metal oxides

1. INTRODUCTION

To meet the growing global energy demands and mitigate the considerable greenhouse gas emissions resulting from the extensive use of fossil fuels, an urgent and widespread transition from conventional technologies to more sustainable and efficient energy conversion technologies is crucial [1]. Among the various alternatives, fuel cells emerge as a promising eco-friendly energy conversion technology, positioned to play a substantial role in the future global energy scenario [2,3]. Fuel cells offer distinct benefits, encompassing heightened energy conversion efficiency, minimal environmental impact due to reduced emissions, adaptability across various applications, scalable design to accommodate diverse energy needs, and subdued operational noise levels [4]. Despite the notable advantages they offer, the current dependency on expensive and scarce Pt catalysts in fuel cells presents a significant drawback, particularly, due to the slow reaction kinetics characterizing the ORR, a key process in fuel cells [5]. This reliance on precious metals, renders the production of fuel cells economically prohibitive for a diverse array of uses. As a result, there exists a pressing need to discover and advance alternative catalyst materials that can effectively catalyze the ORR, offering a more cost-effective and sustainable solution for the widespread adoption of fuel cell technology.

One of the promising alternatives emerged as the substitution of platinum-based catalysts is the nonprecious transition metal catalysts. Within this context, several non-noble metal-based electrocatalysts have been thoroughly explored. Examples of these include transition-group metal oxides, metal sulfides, single-atom metals [6–9], metal selenides [10–12], metal organic frameworks [13], and layered double hydroxides (LDHs) [14]. These materials have been extensively utilized and surveyed to be promoted as alternatives to Pt-based catalysts. Another important attempt is to incorporate these materials with other carbon-based novel surfactant materials like graphene [15,16], Carbon nano-tubes [17], graphitic carbon nitride [18], and Mxene [19]. In this regard, Mousavi et al., [20] synthesized and electrochemically assessed a dual-functional hybrid material by integrating lanthanides into ZIF for ORR electrocatalyst and supercapacitor applications. In another study, Pakzad et al., [21] assessed the performance of a new nanocomposite comprised of Cerium doped graphitic carbon nitride and cobalt oxide as a dual-functional advanced material for ORR catalyst and electrode material for supercapacitors. Hosseini et al. [22] conducted an assessment of the ORR electrocatalytic performance of a novel hybrid nanocomposite. This composite consists of LDH-derived CoNiMn mixed metal oxide nanoflakes, which are adorned on a substrate of reduced graphene oxide that has been doped with single atoms of cobalt and nitrogen. Hu et la. [23], synthesized carbon supported non-precious metals by a facile zinc-mediated pyrolysis process and studied their ORR activity. The study results revealed that the preferred four-electron ORR activity can be ranked as follows: carbon-supported Cu > Co > Mn > Fe > Ni. Yang et al. [24] introduced additional carbon defects into N-doped MOF-derived carbon polyhedron through NaCl/KCl-assisted pyrolysis to tailor the ORR performance of FeCo bimetallic catalysts.

In this research endeavor, we have successfully created a new hybrid catalyst designed for the ORR. This electrocatalyst combines a triple Metal Oxide (IIIMO), with a porous graphitic carbon nitride (PCN) substrate. To our knowledge, this is the first attempt to synthesize and electrochemically assess the effectiveness of a triplex metal oxide incorporated onto Porous Graphitic Carbon Nitride for catalyzing the ORR.

2. EXPERIMENTAL SECTION

2.1. Materials

Urea (CH_4N_2O), methanol (CH_3OH), ethanol (C_2H_6O), Potassium Hydroxide (KOH), Cobalt Nitrate Hexahydrate ($Co(NO_3)_2\bullet6H_2O$), Nickel Nitrate Hexahydrate ($Ni(NO_3)_2\bullet6H_2O$), Manganese Nitrate Tetrahydrate ($Mn(NO_3)_2\bullet4H_2O$), Nafion solution (5 wt.%) ($C_7HF_{13}O_5S\bullet C_2F_4$), Sodium Hydroxide (NaOH), and Sodium Carbonate (Na_2CO_3). All materials were supplied by Merck (Germany) and Sigma-Aldrich (USA).

2.2. Synthesis Methods

In this study, a new nanocomposite consisting of Triple (CoNiMn) Metal Oxide (IIIMO) and porous graphitic carbon nitride (PCN) was synthesized. The synthesis process entailed the separate synthesis of PCN and IIIMO, followed by the incorporation of IIIMO onto the PCN. The IIIMO was obtained through the calcination of CoNiMn-LDH derived from the coprecipitation of metal salts (cobalt, nickel, and manganese nitrates), as detailed in a separate publication [22].

To synthesize PCN, we adopted a straightforward one-pot calcination method to synthesize PCN as outlined by Guo et al. [25]. Initially, 25 grams of urea were dispersed in 25 milliliters of deionized water at 50°C, resulting in a transparent aqueous urea solution. Subsequently, the solution was transferred to a covered 50-milliliter alumina crucible and enclosed with aluminum foil. The sealed precursor was then exposed to temperatures of 600°C within a muffle furnace, following a heating ramp rate of 5°C per minute, for a duration of 6 hours. Afterward, the product was allowed to cool naturally to room temperature, yielding a final light-yellow product referred to as PCN.

A facile single-step method was employed to assemble the IIIMO onto PCN using a layer-by-layer assembly approach [26]. In essence, 100 mg of the as-synthesized PCN were dissolved in 20 milliliters of methanol and subjected to continuous stirring for a duration of one hour. Following this, a specific quantity of IIIMO was introduced into the colloidal PCN solution. The resulting solution was stirred for 12 hours, after which it was transferred to a vacuum oven for drying. Various samples of PCN-IIIMO were obtained using the same procedure with different weight ratios of IIIMO (10%, 20%, 50%, and 100% by weight) to PCN, resulting in samples designated as PCN-IIIMO10%, PCN-IIIMO20%, PCN-IIIMO50%, and PCN-IIIMO100%.

2.3. Characterization

The synthesized nanocomposites were assessed and discussed by using several characterization approaches as below:

- XRD (X-ray diffraction) analysis using a Rigaku Ultima IV instrument with copper Kα radiation.
- FESEM (field emission scanning electron microscope) examination with a JSM-7100F device
- EDS (Energy Dispersive Spectroscopy) analysis for elemental composition.
- FTIR (Fourier transform infrared spectroscopy) recorded using a Bruker Tensor27 instrument.

Moreover, for electrochemical measurements, a three-electrode setup with an Autolab PGSTAT204 Potentiostat was employed. The work electrode was a 2mm GC (glassy carbon), supported the catalyst ink, and was linked to a Rotating Disk Electrode (RDE) under the speed regulation of a BHP 2090 controller. The reference and counter electrodes utilized were Ag/AgCl (in KCl) and a graphite rod, respectively. To assess the electrochemical performance of the synthesized materials, a catalyst ink was meticulously prepared. To this aim, 2 mg of the synthesized catalyst was dispersed in a solution composed of ethanol, water, and 5 wt.% nafion. The work electrode was then coated with 6 µl of this ink, yielding a catalyst loading of 0.4 mg/cm². This carefully designed setup allowed for precise electrochemical investigations and evaluations of the catalyst's performance.

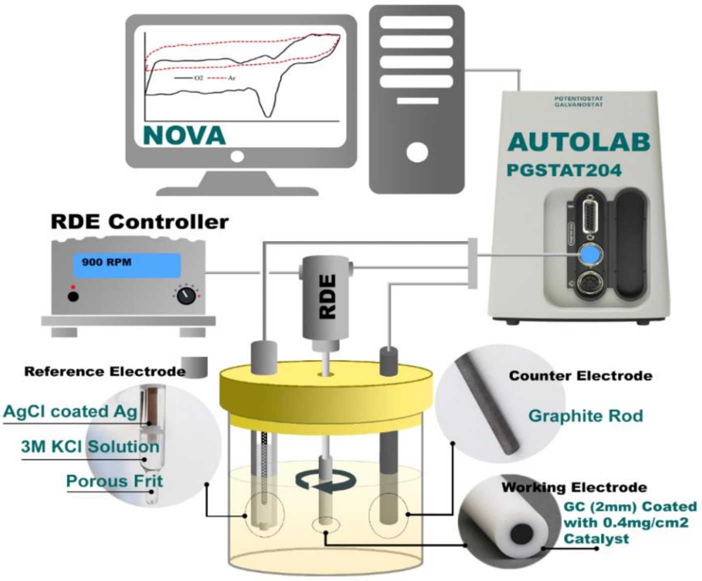

Figure 1. Schematic of the conducted three-electrode setup for electrochemical measurements

Four electrochemical measurements were conducted to assess ORR performance:

- Cyclic Voltammetry (CV) with a scanning rate of 10 mV/s (-1 V to 0.2 V)
- Linear Sweep Voltammetry (LSV) at different rotational speeds (400, 625, 900, 1225, 1600 and 2025 rpm) with a scanning rate of 10 mV/s (-1 V to 0.2 V)
- Koutecký–Levich (K-L) analysis extracted from LSV curves
- Chronoamperometry at -0.6V and 1600 rpm rotation speed

All measurements used a 0.1 M KOH aqueous solution purged with pure O_2, and we replicated CV trials with Ar-saturated electrolyte for selectivity. Figure 1 shows the schematic illustration of the conducted electrochemical measurements.

To assess the electron transfer pathways (2 or 4 electrons) of the catalysts synthesized in this investigation under alkaline conditions, the analysis utilized K-L relationships. These relationships offer a method for computing the electron transfer number (n) through the following mathematical analysis:

$$\mathrm{j}^{-1} = \mathrm{j}_k^{-1} + \aleph^{-1}\mathcal{E}^{-0.5} \tag{1}$$

where j represents the total current density, j_k signifies the kinetic limiting current density, $\mathcal{E}$ denotes the electrode rotation rate in revolutions per minute (rpm), and the parameter $\aleph$ can be derived through the gradient of the K-L plots. This coefficient facilitates the determination of the electron transfer number (n) by means of the subsequent equation:

$$\aleph = 0.2\mathrm{nFC_bC_d}^{2/3}\eta^{-1/6} \tag{2}$$

In the above Equation, n stands for the number of electron transfer, F represents the Faraday constant (96485 $\mathrm{Cmol^{-1}}$), $\mathrm{C_b}$ is the bulk concentration of oxygen molecules (1.2×10^{-6} mol $\mathrm{cm^{-3}}$), $\mathrm{C_d}$ denotes the diffusion coefficient of oxygen molecule in 0.1 M KOH (1.9×10^{-5} $\mathrm{cm^2s^{-1}}$), and η represents the kinetic viscosity (0.01 $\mathrm{cm^2s^{-1}}$).

In an alkaline environment, the ORR proceeds via two separate routes: a two-electron pathway and a four-electron pathway, outlined as follows:

$$\text{2 electron pathway: } \mathrm{O_2 + H_2O + 2e^- \rightleftharpoons HO_2^- + OH^-} \tag{3}$$

$$\mathrm{HO_2^- + H_2O + 2e^- \rightleftharpoons 3OH^-}$$

$$\text{4 electron pathway: } \mathrm{O_2 + 2H_2O + 4e^- \rightleftharpoons 4OH^-} \tag{4}$$

The four-electron pathway is commonly regarded as the ideal pathway, offering superior efficiency.

3. RESULTS AND DISCUSSION

3.1. Characterization and morphology studies

3.1.1. FESEM

The examination of the prepared samples, including PCN, IIIMO, PCN-IIIMO10%, PCN-IIIMO20%, PCN-IIIMO50%, and PCN-IIIMO100%, involved a thorough investigation of their morphologies using FESEM, as illustrated in Figure 2. In Figure 2a, the highly-porous nature of the synthesized PCN is prominently displayed, aligning well with the structure previously documented by [25]. Notably, the FESEM image of IIIMO (Figure 2b) reveals an uneven and asymmetrical configuration, arising from the unbalanced and disorderly dispersion of diverse metal, bimetal, and tri-metal oxides. The subsequent Figures 2(c-f) offer a comprehensive view of the successful integration of IIIMO nanoparticles onto the PCN porous structure. This integration is evident in the morphological changes observed in the images, signifying the effective combination of the two components. However, a discernible concern arises in the case of PCN-IIIMO50% and PCN-IIIMO100%, where stacking and agglomeration of metal oxide particles are observed. This phenomenon represents an unfavorable factor, potentially impacting the overall performance of the composite material. Further insights into addressing these stacking and agglomeration issues could contribute significantly to enhancing the overall quality of the synthesized materials.

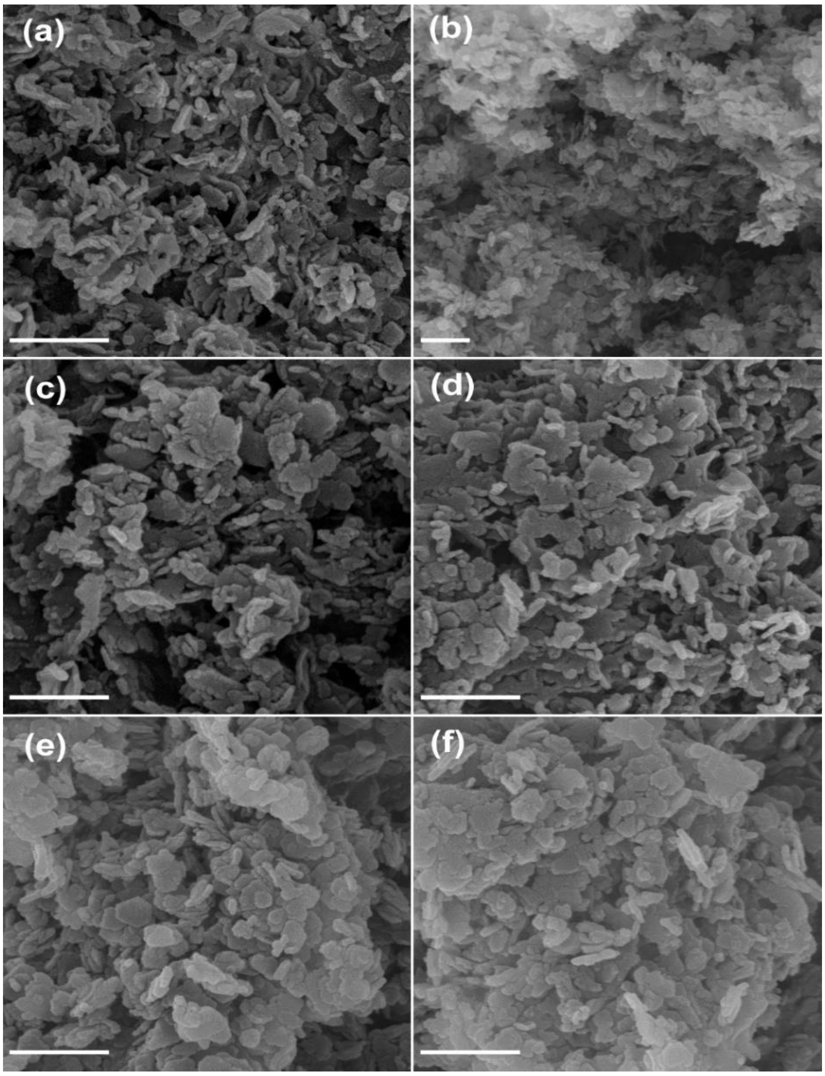

Figure 2. The FESEM images of (a) PCN, (b) IIIMO, (c) PCN-IIIMO10%, (d) PCN-IIIMO20%, (e) PCN-IIIMO50% and (f) PCN-IIIMO100%, scale bar 500 nm

3.1.2. EDS – Elemental Mapping

The investigation of synthesized samples involved the use of Energy Dispersive X-ray Spectroscopy (EDS) analysis to examine the presence of various atoms within their structures. EDS analysis proves particularly valuable for assessing the weight percentage of atoms in composite materials. Table 1 presents the EDS analysis results for PCN, IIIMO, PCN-IIIMO10%, PCN-IIIMO20%, PCN-IIIMO50%, and PCN-IIIMO100%. The color elemental mapping composition of these samples is visually depicted in Figure 3.

In the case of PCN, the highest weight percentage was associated with Nitrogen (57%) and Carbon (33%) elements, while Oxygen elements constituted a minor presence (10%). This elemental composition aligns well with findings reported in other literature [27]. The existence of oxygen within the PCN framework may be ascribed to oxygen functionalization during the synthesis process in an open-air furnace or the existence of surface-adsorbed water in the PCN.

Analyzing IIIMO via EDS confirmed the presence of Co (28.1%), Mn (23.2%), and Ni (11.4%) elements, with minor amounts of C (3.1%) and a significant presence of O (34.2%). This is attributed to carbonate ions remaining from the LDH calcination process and oxidation of metallic ions, respectively.

Furthermore, the uniform distribution of metal atoms alongside C, N, and O atoms in PCN-IIIMO composites was evident. Notably, the percentage of metal atoms approximately mirrored the composite ratio of IIIMO in the PCN-IIIMO composites. As IIIMO increased in the PCN-IIIMO composite, the weight percentages of metal atoms also increased. This uniform distribution of constituent elements was consistently observed across all samples.

Table 1. The EDS analysis results of (a) PCN, (b) IIIMO, (c) PCN-IIIMO10%, (d) PCN-IIIMO20%, (e) PCN-IIIMO50% and (f) PCN-IIIMO100%

	Weight percentages						
Sample	C%	O%	N	Co	Mn	Ni	sum
PCN	33	10	57	-	-	-	
IIIMO	3.1	34.2	-	28.1	23.2	11.4	100
PCN-IIIMO10%	30.8	13.2	49.8	2.7	2.3	1.2	100
PCN-IIIMO20%	27.2	15.5	45.7	4.9	4.5	2.2	100
PCN-IIIMO50%	22.3	19.1	36.6	9.2	8.2	4.6	100
PCN-IIIMO100%	16.3	23.2	26.3	14.9	12.4	6.9	100

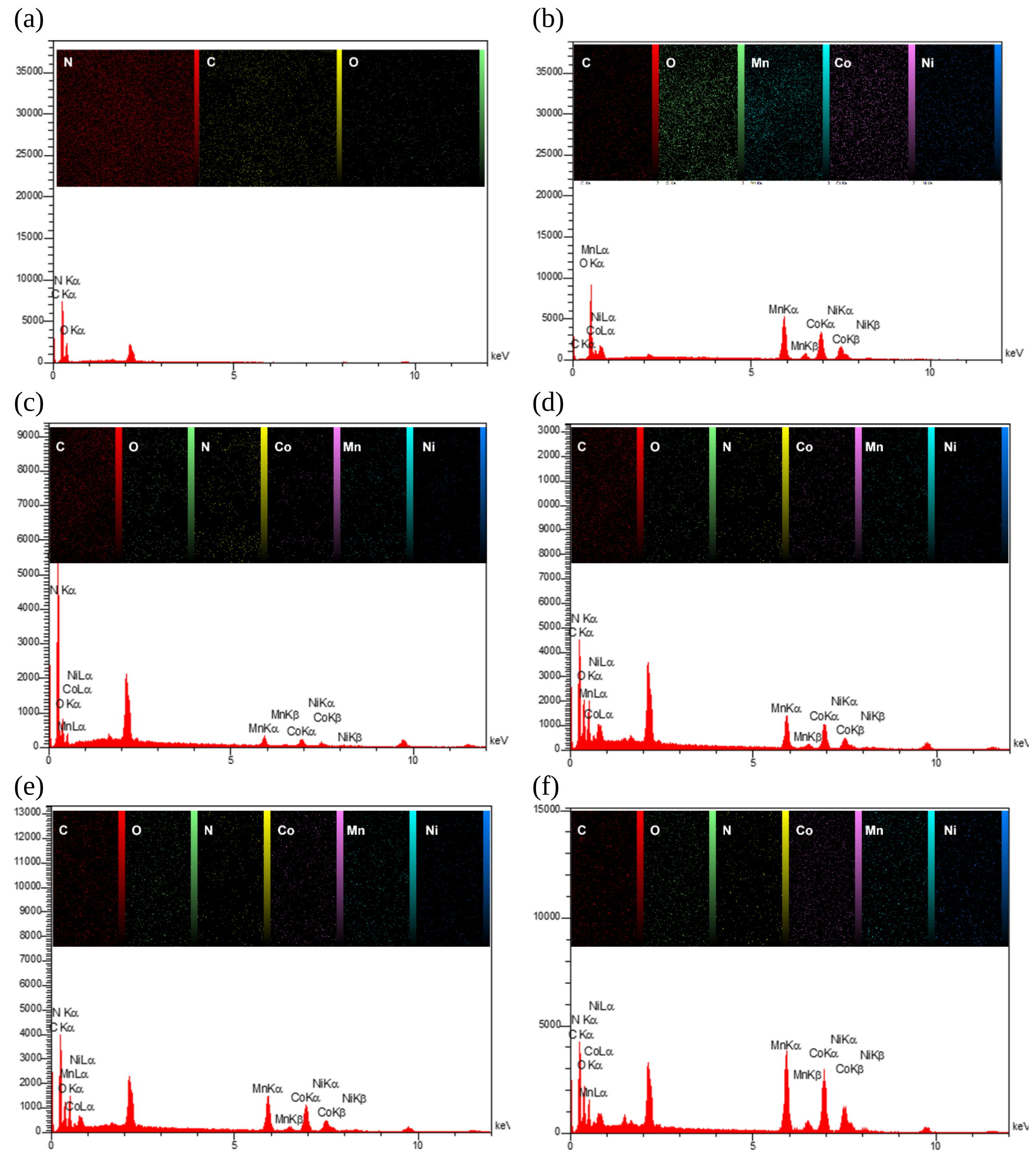

Figure 3. EDS and Elemental Mapping results of (a) PCN, (b) IIIMO, (c) PCN-IIIMO10%, (d) PCN-IIIMO20%, (e) PCN-IIIMO50% and (f) PCN-IIIMO100%

3.1.3. XRD

To examine the crystal phase of the prepared catalysts, we employed XRD, a highly valuable technique in materials science. XRD offers a comprehensive assessment of the crystalline phases present within a material while simultaneously providing essential information about its chemical composition. Moreover, XRD serves as an invaluable tool for confirming the structural characteristics of synthesized materials. Figure 4 displays the XRD patterns obtained from the synthesized samples, shedding light on the intricate crystalline structures present within them. When examining the XRD patterns of PCN, the emergence of two distinct peaks can be discerned. Specifically, a relatively faint peak at 13.1 degrees (100) and a considerably intense peak at 27.7 degrees (002) are readily evident. These peaks are ascribed to the presence of the tri-s-triazine ring structure and the interlayer spacing of graphitic carbon nitride, respectively [21,25].

In the case of the IIIMO, the XRD patterns closely correspond to previously reported patterns of various metal oxides, including Co_3O_4, $MnCo_2O_4$, MnO, MnO_2, Mn_2O_3, $NiCo_2O_4$, and NiO [22]. These correspondences align with references such as (JCPDS 42-1467) [28,29], (JCPDS 23-1237) [28], (JCPDS 00-075-1090) [30], (JCPDS 44-0141) [31], (JCPDS 41-1442) [32], (JCPDS 73-1702) [33], and (JCPDS 01-073-1519) [34,35], respectively.

It is noteworthy that the XRD patterns of PCN-IIIMO exhibit peaks that closely resemble those identified in both the XRD pattern of IIIMO and that of PCN.

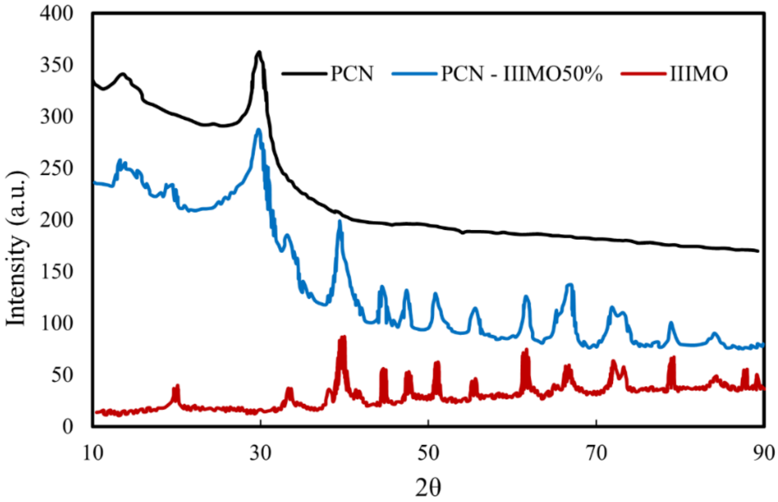

Figure 4. The XRD patterns of the synthesized PCN, IIIMO, and PCN-IIIMO50%

3.1.4. FTIR

The investigation of the chemical bonds within the synthesized samples has been conducted using the FTIR technique, a powerful analytical tool providing valuable insights into the material's chemical properties. The FTIR results for the fabricated samples are illustrated in Figure 5. Utilizing FTIR analysis allows for the identification of various materials. Figure 5 demonstrates that plain PCN exhibits various peaks. The absorption peak at 807 cm^{-1} corresponds to the N–H bonds' deformation related to the out-of-plane bending mode of the tri-s-triazine ring units, indicating the existence of graphitic carbon nitride structure. The wide peak within the span of 3000–3500 cm^{-1} is ascribed to the terminal –NH2 or =NH groups. Additionally, the broad peak within the 1200–1700 cm^{-1} range is assigned to the stretching vibration modes of nitrogen-containing heterocyclic rings (N – C= N) [25]. In the FTIR spectrum of the PCN-IIIMO composite, the same peaks observed in plain PCN are present.

Furthermore, an additional broad peak, located at wavenumbers below 800 cm^{-1}, is evident. This peak is associated with the overlapping vibrations of metal-oxide and metal hydroxide. The appearance of this peak indicates the incorporation of metal components into the PCN structure, providing valuable information about the composite material's composition.

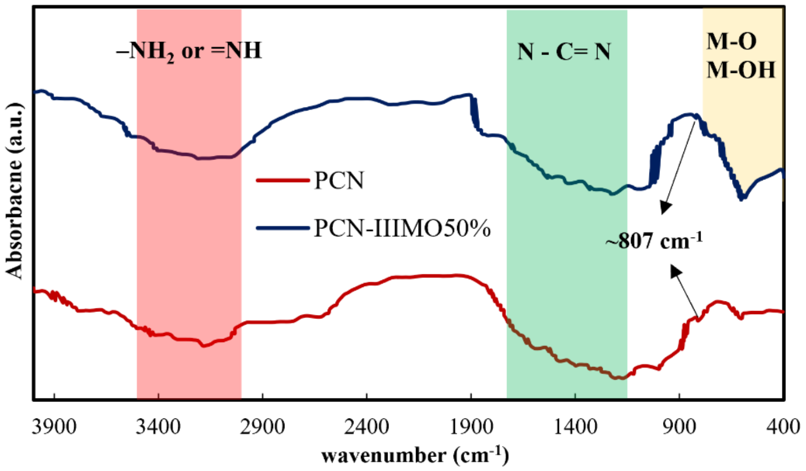

Figure 5. The FTIR spectra of the pristine PCN, and PCN-IIIMO composite

3.2. Electrochemical Characterization

To assess the performance of the synthesized electrocatalysts for ORR applications, it is crucial to investigate their electroactivity. To this aim, four voltammetry analyses; namely, CV, LSV, K-L, and chronoamperometry, were employed to scrutinize the electrocatalytic performance of the synthesized materials in a 0.1 M KOH aqueous solution saturated with either oxygen (as a fuel) or argon (as inert gas).

3.2.1. Cyclic Voltammetry (CV)

Figure 6 illustrates the CV tests conducted on PCN, IIIMO, PCN-IIIMO10%, PCN-IIIMO20%, PCN-IIIMO50%, and PCN-IIIMO100%. The dashed-red and black curves represent the CV analysis results of the prepared samples in O_2- and Ar-saturated electrolytes, respectively. Notably, all synthesized electrocatalysts exhibited an ORR peak (sharp reduction peak) during the CV tests in the O_2-saturated medium, indicating their catalytic activity in an alkaline solution. Additionally, a smooth cycle was noted for all catalysts in the Argon-purged KOH solution, indicating the lack of undesirable activity peaks under these conditions. A desirable ORR catalyst demonstrates a tendency to specifically catalyze the reduction of oxygen while suppressing the generation of other undesired byproducts. Furthermore, the current density was found to be highest in PCN-IIIMO20%, in comparison to bare PCN and IIIMO. This enhancement is attributed to the synergistic improvement of electrochemical properties within the PCN-IIIMO composite. The outcomes highlight the potential of PCN-IIIMO20% as a promising electrocatalyst for ORR applications.

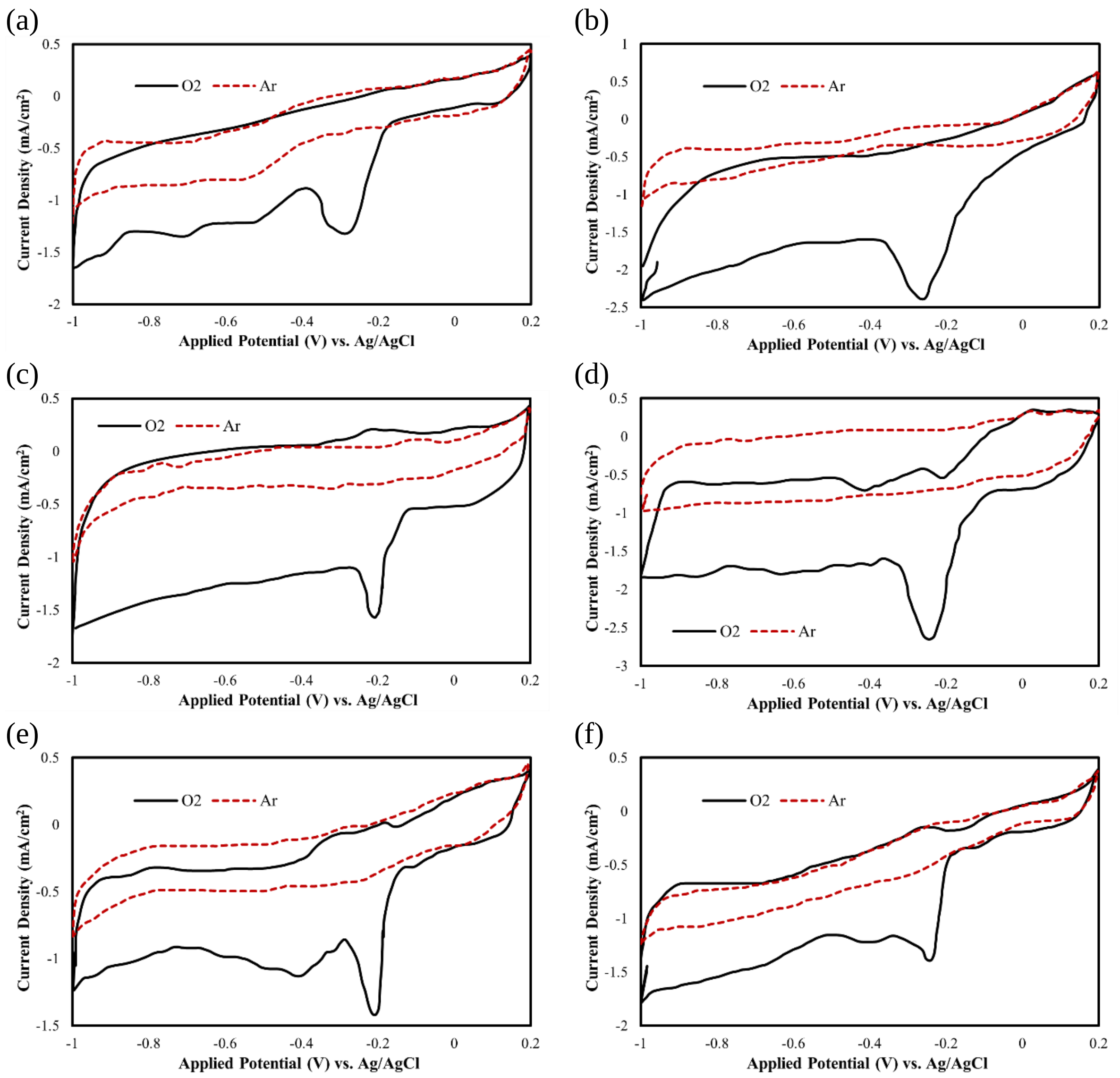

Figure 6. CV curves of (a) PCN, (b) IIIMO (c) PCN-IIIMO10%, (d) PCN-IIIMO20%, (e) PCN-IIIMO50%, and (f) PCN-IIIMO100%

3.2.2. Linear Sweep Voltammetry (LSV)

To delve deeper into the catalytic performance and kinetics of the synthesized catalysts, we carried out the LSV tests using a RDE device in an oxygen-purged 0.1 M KOH alkaline medium. The tests were performed at several RDE speeds, and the related plots are shown in Figure 7. As depicted in Figure 7, in all the samples, it is evident that as the rotation speed increases, there is a noticeable increment in the absolute value of the current density. Essentially, the higher rotational speed ensures a more abundant oxygen supply to the surface of the work electrode, where the catalyst ink is placed. Accordingly, this escalation in rpm contributes to an elevated electron transfer and current values. From the LSV curves, two key factors are discerned: the onset potential and electron transfer number. In electrochemistry, the onset potential refers to the potential at which a particular electrochemical reaction initiates.

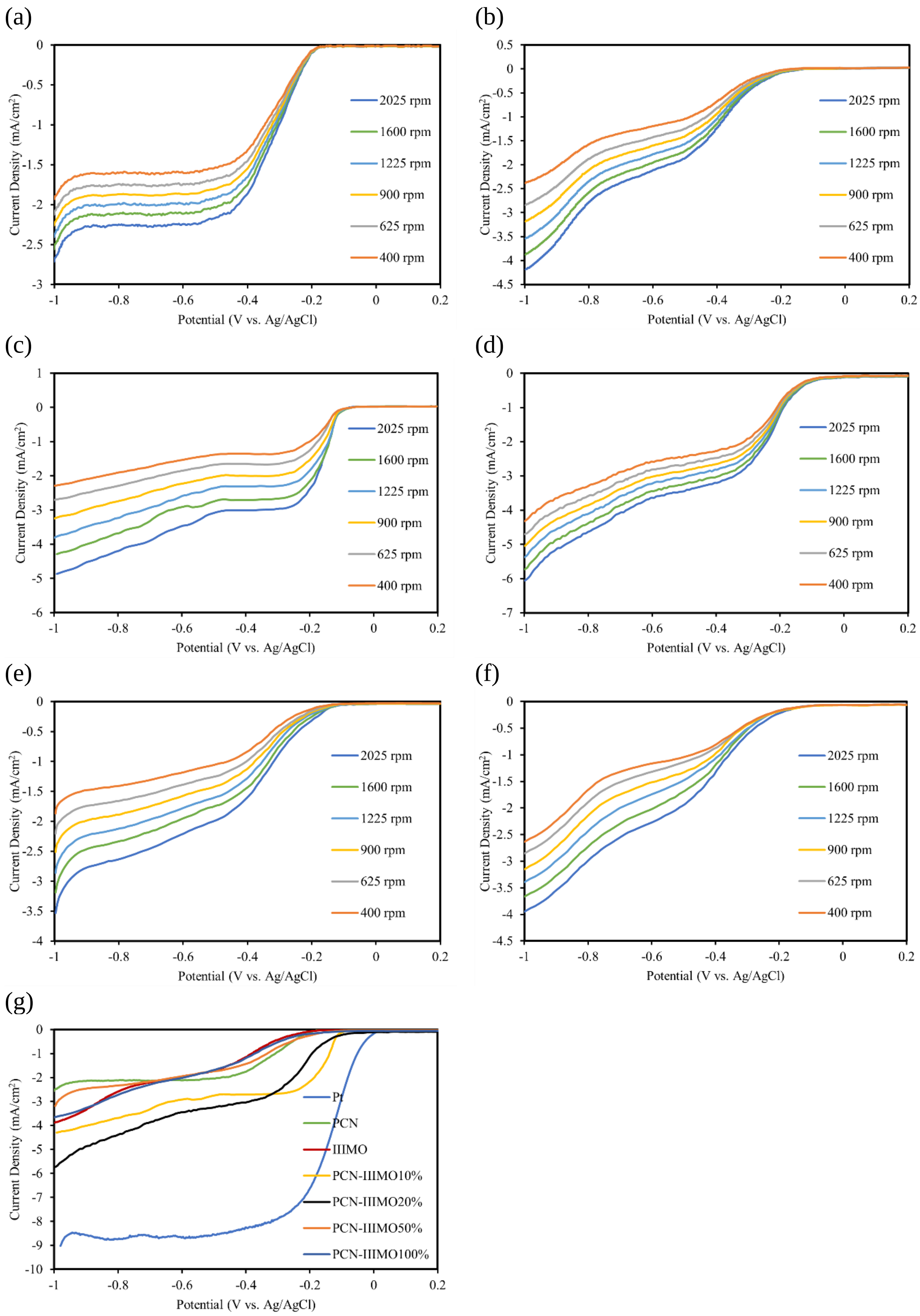

Figure 7. LSV Plots at several RPMs of (a) PCN, (b) IIIMO (c) PCN-IIIMO10%, (d) PCN-IIIMO20%, (e) PCN-IIIMO50%, (f) PCN-IIIMO100%, and (g) LSV of the samples at 1600 rpm along with commercial 20% Pt/C electrocatalyst

Onset potentials with more positive values (approaching to zero) suggests improved kinetics for the ORR. The LSV curves reveal that PCN-IIIMO20% exhibited a significantly improved onset potential (-0.09 V) compared to pure PCN (-0.18 V), IIIMO (-0.17 V), PCN-IIIMO10% (-0.12 V), PCN-IIIMO50% (-0.13 V) and PCN-IIIMO100% (-0.15 V). It's important to highlight that the recorded current densities for the samples exhibited in a decreasing sequence as PCN-IIIMO20% > PCN-IIIMO10% > IIIMO > PCN-IIIMO100% > PCN-IIIMO50% > PCN. Notably, IIIMO and PCN alone demonstrated insufficient electrocatalytic performance for the ORR.

To facilitate comparison, Figure 7g presents the LSV plots of each sample at 1600 RPM alongside a commercially available Pt/C catalyst. A transition to more favorable onset potentials and increased current densities is evident, with the sequence from IIIMO and PCN to PCN-IIIMO100%, PCN-IIIMO50%, PCN-IIIMO10% and PCN-IIIMO20%. Sample PCN-IIIMO20% exhibits a notably enhanced onset potential (-0.09 V) and increased current densities when compared to other samples. The enhanced onset potential in PCN-IIIMO20% is a result of the active sites created through the synergistic interaction between graphitic carbon nitride and triple metal oxide particles. This interaction boosts the electrochemical properties of the final product and promotes the role of metal oxides as active sites within the graphitic carbon nitride structure. This collaboration between the two components contributes to the improved onset potential. It is essential to emphasize that an increase in the proportion of triple metal oxides in PCN did not invariably result in improved electrochemical performance. Excessive or insufficient amounts can accumulate and reduce the availability of active sites, impacting overall performance. Figure 7 illustrates this phenomenon, highlighting that the optimal concentration of IIIMO in PCN, as determined by the onset potential and highest current density, is 20%.

3.2.3. K-L method

A crucial aspect illuminated by the LSV analysis of electrocatalysts is the determination of the number of electron transfer. Utilizing the Koutecký–Levich (K-L) method, as described by Equation 1 and Equation 2, electron transfer data was extracted from the LSV results and is visually represented in Figure 8. Examination of Figure 8 reveals that the computed average electron transfer numbers for PCN, IIIMO, PCN-IIIMO10%, PCN-IIIMO20%, PCN-IIIMO50%, and PCN-IIIMO100% are 2.68, 2.71, 2.9, 3.27, 2.84, and 2.73, respectively. In pursuit of an ideal ORR, characterized by a four-electron transfer mechanism resulting in the production of $4OH^-$ (as depicted in Equation 4), it is noteworthy that the PCN-IIIMO20% composite exhibits an electron transfer number of 3.27. This suggests a remarkable proximity to the optimal four-electron transfer mechanism, indicating a high efficacy in ORR. The heightened electron transfer number of PCN-IIIMO20% underscores its commendable electrocatalytic performance. The infusion of triple metal oxides into the porous graphitic carbon nitride structure is responsible for a substantial increase of 0.59 in the electron transfer number noticed in PCN-IIIMO20%, surpassing the values for pure PCN and IIIMO. This incorporation of triple metal oxides imparts enhanced electrical conductivity and an expanded surface area, leveraging the distinctive configuration of PCN. The noteworthy enhancement in the electron transfer number in PCN-IIIMO20% is attributed to the optimized quantity of IIIMO within the PCN-IIIMO composite, harnessing the advantages of both the high porosity of the PCN structure and the superior electrochemical properties of the metal oxide species in IIIMO.

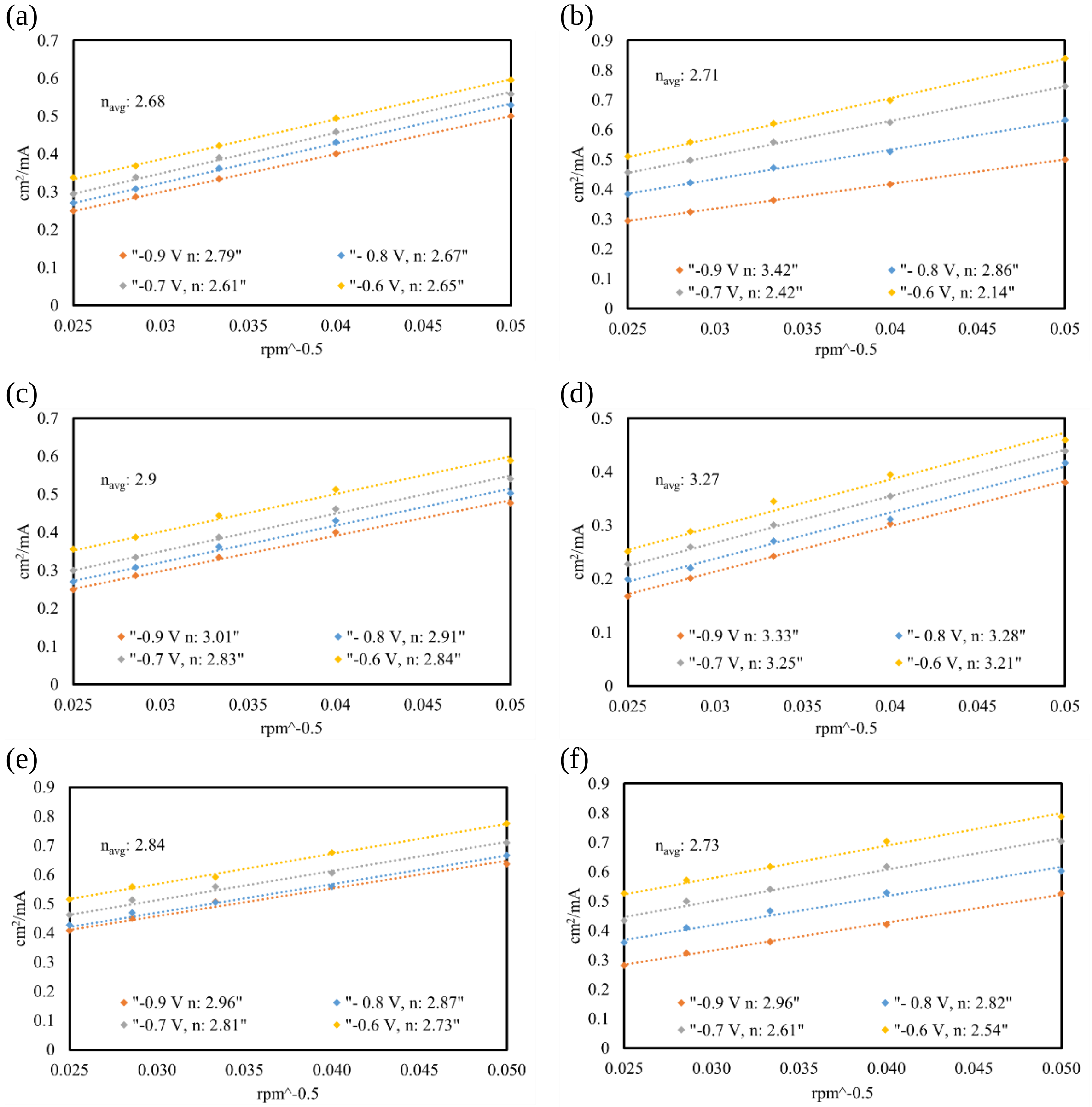

Figure 8. K-L plots of (a) PCN, (b) IIIMO, (c) PCN-IIIMO10%, (d) PCN-IIIMO20%, (e) PCN-IIIMO50%, (f) PCN-IIIMO100%

3.2.4. Chronoamperometry

Figure 9 illustrates chronoamperometric analyses conducted on the synthesized electrocatalysts, providing a valuable insight into their durability. Employing a constant voltage of -0.6 V, the electrochemical cell underwent a 7200-second analysis. In Figure 9, the relative current for PCN, IIIMO, and PCN-IIIMO20% is depicted, showing values of 81%, 79%, and 80%, respectively. A higher current retention indicates enhanced stability and durability over time. The decline in current over time is expected, attributed to the gradual corrosion of PCN, inevitable dissolution, and aggregation of IIIMO nanoparticles during the reactions, leading to a reduction in the electrochemically active surface area. Notably, PCN demonstrates superior durability compared to IIIMO and PCN-IIIMO20%, as metal oxide nanoparticles exhibit faster degradation during electrochemical reactions than the pristine PCN. It's noteworthy that the composite PCN-IIIMO20% exhibits higher current retention after 7200 seconds compared to pure IIIMO. This can be attributed to the presence of PCN in its structure. Additionally, when IIIMO nanoparticles are combined with PCN, as a porous graphitic structure, it helps prevent the agglomeration of metal oxide particles by linking the metal clusters onto the PCN structure, contributing to enhanced durability.

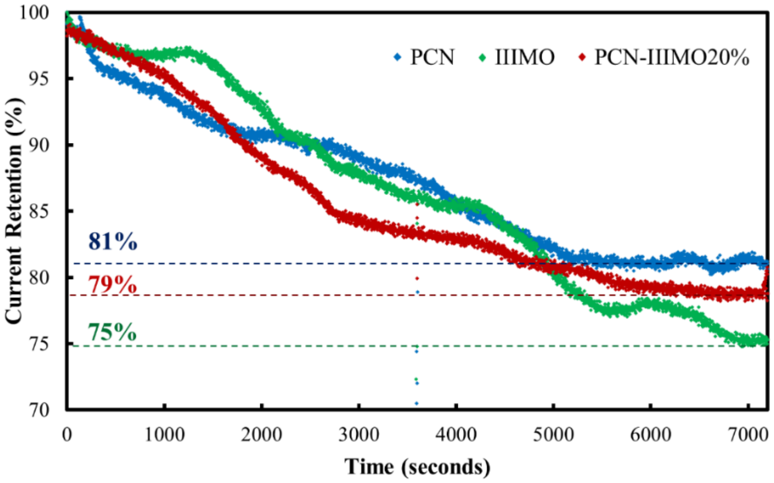

Figure 9. Chronoamperometry experiments, current density retention versus time of PCN, IIIMO, PCN-IIIMO20%, under continuous operation for 7200 seconds, 1600 rpm, in an oxygen-purged 0.1 M KOH solution

4. CONCLUSION

In conclusion, this study focused on addressing the imperative need for efficient and cost-effective non-precious electrocatalysts to propel advancements in energy conversion and storage systems. The synthesized hybrid electrocatalyst, PCN-IIIMO, Triple Metal Oxide (IIIMO) decorated on a porous graphitic carbon nitride (PCN), demonstrated promising physiochemical and electrochemical performance for the ORR. The composite exhibited a synergistic enhancement of catalytic activity for the ORR, leveraging its binary composition and hierarchically porous structure. The layer-by-layer assembly method used in the synthesis, incorporating various weight ratios of IIIMO (10, 20, 50, and 100%), proved effective in tailoring the electrocatalyst's properties. Physiochemical analyses verified the successful combination of the as-synthesized IIIMO with the PCN lattice. Notably, electrochemical analyses highlighted the superior performance of PCN-IIIMO20%, showcasing an onset potential of -0.09 V, an electron transfer number of 3.3, and an impressive current retention durability of 79% after 7200 seconds of continuous operation. This underscores the practical viability of the PCN-IIIMO composite as a robust and efficient electrocatalyst for ORR applications.

Our findings contribute to the ongoing efforts to develop environmentally friendly and economically viable advanced materials for sustainable energy technologies. The success of the PCN-IIIMO composite in enhancing ORR catalytic performance opens avenues for further research and development in the quest for greener and more efficient energy conversion and storage solutions. Future research endeavors could focus on the exploration of various non-precious metal species, encompassing oxides, nitrides, and single atoms for integration onto carbon-based materials as efficient ORR electrocatalysts.

Acknowledgments

This work is based upon research funded by Iran National Science Foundation - Project No. 4013348.

Declarations of interest

The authors declare no conflict of interest in this reported work.

REFERENCES

[1] H. Forootan Fard, M. Khodaverdi, F. Pourfayaz, and M.H. Ahmadi, Int. J. Hydrogen Energy 45 (2020) 25307.

[2] S.S. Hosseini, M. Mehrpooya, A.S. Alsagri, and A.A. Alrobaian, Energy Convers. Manag. 197 (2019) 111878.

[3] M. Mehrpooya, and S.S. Hosseini, Int. J. Hydrogen Energy 50 (2024) 388.

[4] M. Khodaverdi, F. Pourfayaz, and M. Mehrpooya, Fuel Cells 21 (2021) 172.

[5] H. Kowsari, M. Mehrpooya, and F. Pourfayaz, Int. J. Hydrogen Energy 45 (2020) 27129.

[6] Q. Zhang, X. Zhang, J. Wang, and C. Wang, Nanotechnology 32 (2020) 032001.

[7] G. Han, Y. Zheng, X. Zhang, Z. Wang, Y. Gong, C. Du, M.N. Banis, Y.M. Yiu, T.K. Sham, L. Gu, Y. Sun, Y. Wang, J. Wang, Y. Gao, G. Yin, and X. Sun, Nano Energy 66 (2019) 104088.

[8] L. Li, Y.J. Chen, H.R. Xing, N. Li, J.W. Xia, X.Y. Qian, H. Xu, W.Z. Li, F.X. Yin, and G.Y. He, Nano Res. 15 (2022) 8056.

[9] Z. Du, X. Chen, W. Hu, C. Chuang, S. Xie, A. Hu, W. Yan, X. Kong, X. Wu, H. Ji, and L.J. Wan, J. Am. Chem. Soc. 141 (2019) 3977.

[10] J. Ding, S. Ji, H. Wang, V. Linkov, and R. Wang, J. Power Sources 423 (2019) 1.

[11] Y.S. Chao, D.S. Tsai, A.P. Wu, L.W. Tseng, and Y.S. Huang, Int. J. Hydrogen Energy 38 (2013) 5655.

[12] N.S. Arul, and J.I. Han, Mater. Lett. 181 (2016) 345.

[13] S.A. Mousavi, and M. Mehrpooya, Energy 214 (2021) 119053.

[14] H. Abedi, and M. Mehrpooya, J. Alloys Compd 875 (2021) 160047.

[15] X. Chen, H. Zhu, J. Zhu, and H. Zhang, Chem. Eng. J. 451 (2023) 138998.

[16] A. Tyagi, Y.K. Penke, P. Sinha, I. Malik, and K.K. Kar, J. Ramkumar, H. Yokoi, Int. J. Hydrogen Energy 46 (2021) 22434.

[17] T. Ren, Y. Lv, H. Zhang, Z. Yang, X. Wu, H. Zhang, X. Zhang, and J. Guo, J. Electroanal. Chem. 940 (2023) 117510.

[18] V.G. Dileepkumar, K.R. Balaji, R. Vishwanatha, B.M. Basavaraja, S. Ashoka, I. M. Al-Akraa, M.S. Santosh, and S. Rtimi, Chem. Eng. J. 446 (2022) 137023.

[19] K. Chaudhary, B. Basha, S. Zulfiqar, S. Yousaf, E.W. Cochran, M.S. Al-Buriahi, M. Farooq Warsi, M. Shahid, Fuel 351 (2023) 128856.

[20] S.A. Mousavi, M. Mehrpooya, and M.R. Ganjali, Int. J. Hydrogen Energy 51 (2024) 787.

[21] P. Pakzad, M. Mehrpooya, F. Pourfayaz, and M.R. Ganjali, Int. J. Hydrogen Energy 48 (2023) 16294.

[22] S.S. Hosseini, M. Mehrpouya, and M.H. Jahangir, Mater. Chem. Phys. 314 (2024) 128838.

[23] H. Hu, G.H. Gao, B.B. Xiao, P. Zhang, and J.L. Mi, Diam Relat. Mater. 134 (2023) 109776.

[24] K. Yang, Y. Cheng, Y. Lei, Q. Yang, X. Liu, T. Lu, H. Xie, J. Li, T. Zan, and H. Wang, J. Solid State Chem. 329 (2024) 124401.

[25] J. Guo, Y. Sun, R. Xiang, H. Yu, Z. Chen, F. Zhang, and F. Liu, Colloids Surf. A Physicochem. Eng. Asp. 671 (2023) 131600.

[26] M. Tahir, and R. Mansoor, J. Alloys Compd 947 (2023) 169457.

[27] S.K. Lakhera, R.T. Pangal, H.Y. Hafeez, and B. Neppolian, ChemSusChem. 12 (2019) 4293.

[28] D. Wang, X. Chen, D.G. Evans, and W. Yang, Nanoscale 5 (2013) 5312.

[29] R. Nie, J. Shi, W. Du, W. Ning, Z. Hou, and F.S. Xiao, J. Mater. Chem. A Mater. 1 (2013) 9037.

[30] N. Mironova-Ulmane, A. Kuzmin, V. Skvortsova, G. Chikvaidze, I. Sildos, J. Grabis, D. Jankoviča, A. Dindune, and M. Maiorov, Acta Phys. Pol A 133 (2018) 1013.

[31] S.L. Kadam, S.M. Mane, P.M. Tirmali, and S.B. Kulkarni, Current Applied Phys. 18 (2018) 397.

[32] L. Zhang, D. Ge, H. Geng, J. Zheng, X. Cao, and H. Gu, New J. Chem. 41 (2017) 7102.

[33] M. Wu, S. Meng, Q. Wang, W. Si, W. Huang, and X. Dong, ACS Appl. Mater. Interfaces 7 (2015) 21089.

[34] X. Rong, F. Qiu, J. Qin, H. Zhao, J. Yan, and D. Yang, J. Ind. Eng. Chem. 26 (2015) 354.

[35] Y.J. Mai, S.J. Shi, D. Zhang, Y. Lu, C.D. Gu, and J.P. Tu, J. Power Sources 204 (2012) 155.